PROCESSES

Reusable unit process life cycle inventory for manufacturing: high speed laser directed energy deposition

Svenja Ehmsen[1] · Li Yi[1] · Moritz Glatt[1] · Barbara S. Linke[2] · Jan C. Aurich[1]

© The Author(s) 2023

Abstract

The unit process life cycle inventory is a modeling approach to estimate the energy demand and resource requirements of a unit process. Thus, a model of the unit process life cycle inventory for a specific manufacturing process can be used for quantifying the environmental impacts of specific products manufactured by that process. Within the approach, reusable models are developed for specific manufacturing processes. In this paper, the development and validation of a unit process life cycle inventory model for high-speed laser directed energy deposition is presented. This additive manufacturing process offers great potential for the industry due to its fast process speed. However, high-speed laser directed energy deposition has a high energy consumption and resource demand. Assessing the energy demand for individual manufactured products is a time-intensive process that requires expert knowledge. Thus, the development of an adaptable unit process life cycle inventory model enables more convenient assessment and improvement of its energy and resource efficiencies for producing different products. For the development of the model, the subsystems of a high-speed laser directed energy deposition machine are analyzed separately, e. g. the laser generator, the trajectory system, the powder feeder, and the suction system. Afterward, the energy and material demand of these subsystems are described in mathematical models. Finally, the model is validated by comparing the energy demands of three demonstration parts, measured by experiments, and predicted by the model.

Abbreviations

AM	Additive manufacturing
DED	Directed energy deposition
HS DED-LB	High-speed laser directed energy deposition
LCI	Life cycle inventory
UPLCI	Unit process life cycle inventory

Symbols

a	Acceleration (m/s^2)
B	Binary variable (1 if there are turning points, 0 If there are no turning points)
E_e	Total energy consumption of the suction (Wh)
E_l	Total energy consumption of the laser (Wh)
$E_{l,on}$	Energy consumption of the laser while it is switched on (Wh)
$E_{l,ready}$	Energy consumption of the laser while it is ready to fire (Wh)
$E_{l,\ standby}$	Energy consumption of the laser during standby (Wh)
E_{pf}	Total energy consumption of the powder feeder (Wh)
$E_{pf,on}$	Energy consumption of the powder feeder switched on (Wh)
$E_{pf,standby}$	Energy consumption of the powder feeder during standby (Wh)
E_s	Total energy consumption of the peripheral subsystems (Wh)
E_{total}	Total energy consumption (Wh)
E_{ts}	Total energy consumption of the trajectory system (Wh)

✉ Svenja Ehmsen
svenja.ehmsen@mv.uni-kl.de

1 Institute for Manufacturing Technology and Production Systems (FBK), RPTU Kaiserslautern, P.O. Box 3049, 67653 Kaiserslautern, Germany

2 Department for Mechanical and Aerospace Engineering, University of California Davis, 1 Shields Ave, Davis, CA 95616, USA

$E_{ts,on}$	Energy consumption of the trajectory system while it is switched on (Wh)	$P_{pf,on,s,b}$	Basic power consumption of the stirrer of the powder feeder (W)
$E_{ts,on, circle}$	Energy consumption of the trajectory system for a rotationally symmetric scan path (Wh)	$P_{pf,on,s,max}$	Maximum power consumption of the stirrer of the powder feeder (W)
$E_{ts,on, linear}$	Energy consumption of the trajectory system for a rotationally symmetric scan path (Wh)	$P_{pf,standby}$	Power consumption of the powder feeder during standby (W)
$E_{ts,standby}$	Energy consumption of the trajectory system during standby (Wh)	P_s	Power consumption of the peripheral subsystems (W)
l_{layer}	Scan path length per layer (m)	$P_{ts,circle,max}$	Power consumption of the trajectory system for a rotationally symmetric scan path at maximum velocity (W)
$l_{ac/deac}$	Path length to accelerate and decelerate (m)		
$\dot{m}$	Powder mass flow (g/h)	$P_{ts,circle,50\%}$	Power consumption of the trajectory system at 50% maximum speed for a rotationally symmetric scan path (W)
m_{loss}	Powder loss during manufacturing (g)		
$m_{loss,machine}$	Machine-related powder loss (g)		
$m_{loss,process}$	Process-related powder loss (g)	$P_{ts,circle,75\%}$	Power consumption of the trajectory system at 75% maximum speed for a rotationally symmetric scan path (W)
m_{part}	Mass of the manufactured part (g)		
m_{powder}	Powder used during process (g)		
N_{layer}	Quantity of layers (amount)	$P_{ts,linear,ac,max}$	Power consumption of the trajectory system during acceleration to maximum velocity for a rather linear scan path (W)
$N_{path per layer}$	Quantity of single scan path per layer (speed remains unchanged) (amount)		
η_l	Laser efficiency (%)	$P_{ts,linear,ac,min}$	Power consumption of the trajectory system during acceleration to minimum velocity for a rather linear scan path (W)
P_e	Power consumption of the suction system (W)		
$P_{e,b}$	Basic power consumption of the suction system(W)	$P_{ts,linear,deac,max}$	Power consumption of the trajectory system during deceleration from maximum velocity for a rather linear scan path (W)
$P_{e,max}$	Maximum power consumption of the suction system (W)		
$P_{e,50\%}$	Power consumption of the suction system at a suction rate of 50% (W)	$P_{ts,linear,deac,min}$	Power consumption of the trajectory system during deceleration from minimum velocity for a rather linear scan path (W)
$P_{l,max}$	Maximum power consumption of the laser generator (W)		
$P_{l,on}$	Power consumption of the laser generator while it is switched on (W)	$P_{ts,linear,path,max}$	Power consumption of the trajectory system during maintaining the maximum velocity for a rather linear scan path (W)
$P_{l,ready}$	Power consumption of the laser generator while it is ready to fire (W)	$P_{ts,linear,path,min}$	Power consumption of the trajectory system during maintaining the minimum velocity for a rather linear scan path (W)
$P_{l,set}$	Set laser power for processing (W)		
$P_{l,set,max}$	Maximum adjustable laser power (W)	$P_{ts,on,circle}$	Power consumption of the trajectory system for a rotationally symmetric scan path (W)
$P_{l,standby}$	Power consumption of the laser generator during standby (W)		
$P_{pf,on}$	Power consumption of the powder feeder while it is switched on (W)	$P_{ts,on,linear}$	Power consumption of the trajectory system for a rather linear scan path (W)
$P_{pf,on,b}$	Basic power consumption of the powder feeder (W)	$P_{ts,on,linear,ac}$	Power consumption of the trajectory system for a rather linear scan path during acceleration (W)
$P_{pf,on,c}$	Power consumption of the conveyor disc of the powder feeder (W)	$P_{ts,on,linear,deac}$	Power consumption of the trajectory system for a rather linear scan path during deacceleration (W)
$P_{pf,on,c,b}$	Basic power consumption of the conveyor disc of the powder feeder (W)	$P_{ts,on,linear,path}$	Power consumption of the trajectory system for a rather linear scan path during keeping the speed (W)
$P_{pf,on,c,max}$	Maximum power consumption of the conveyor disc of the powder feeder (W)		
$P_{pf,on,s}$	Power consumption of the stirrer of the powder feeder (W)	$P_{ts,standby}$	Power consumption of the trajectory system during standby (W)

Q_c	CROSS-sectional area of the channel in conveyor disc (m^2)
t_{ac}	Acceleration time (h)
$t_{ac,path}$	Time to reach the required speed (h)
t_{deac}	Deacceleration time (h)
$t_{deac,path}$	Time to reduce the speed to change direction (h)
t_{in}	Time for in-step (h)
$t_{l,on}$	Time while laser is switched on (h)
t_{post}	Time for post-step (h)
t_{pre}	Time for the pre-step (h)
$t_{remaining}$	Time to run the remaining acceleration distance and deceleration distance at reached speed (h)
t_{switch}	Total time to switch layers (h)
$t_{switch\ per\ layer}$	Mean time to switch from one layer to another (h)
t_{total}	Total time of one build cycle (h)
t_{track}	Time to run the part geometry at the required speed (h)
$t_{ts,linear,ac,max}$	Time until the maximum velocity of trajectory system is reached (h)
$t_{ts,linear,ac,min}$	Time until the minimum velocity of trajectory system is reached (h)
$t_{ts,linear,deac,max}$	Time until the maximum velocity of trajectory system is decelerated (h)
$t_{ts,linear,deac,min}$	Time until the minimum velocity of trajectory system is decelerated (h)
$t_{ts,on,linear,ac}$	Time until the required velocity of trajectory system is reached (h)
$t_{ts,on,linear,deac}$	Time until the required velocity of trajectory system is decelerated (h)
u_c	Circumference of the channel in the conveyor disc (m)
$\dot{V}_{e,set}$	Set suction volume (m3/h)
$\dot{V}_{e,set,max}$	Maximum suction volume (m^3/h)
$\dot{v}_{i,c}$	Set flow volume carrier gas flow (l/h)
$\dot{v}_{i,s}$	Set flow volume shielding gas flow (l/h)
V_i	Required volume of inert gas (l)
$V_{i,c}$	Required volume of inert gas as carrier gas flow (l)
$V_{i,s}$	Required volume of inert gas as shielding gas flow (l)
$v_{pf,c,set}$	Set conveyor disc speed of the powder feeder (s^{-1})
$v_{pf,c,set,max}$	Maximum conveyor disc speed of the powder feeder (s^{-1})
$v_{pf,s,set}$	Set stirrer speed of the powder feeder (s^{-1})
$v_{pf,s,set,max}$	Maximum stirrer speed of the powder feeder (s^{-1})
v_{ts}	Velocity of trajectory system (m/s)

| $v_{ts,max}$	Maximum velocity of trajectory system (m/s)
ρ_{powder}	Powder density (g/m^3)

1 Background

Additive manufacturing (AM) is used for manufacturing, tooling, and repairing parts with complex geometries. Compared to formative or subtractive manufacturing processes such as milling and casting, AM offers numerous environmental benefits, including the ability to reduce material requirements through lightweight design, limited waste during the manufacturing process, the absence of forming or cutting tools, and improved product performance leading to a more environmentally friendly product usage [1]. However, recent research states that the environmental benefits of AM are not an process-inherent property and must be thoroughly assessed and proven during the design stage [1–3]. This raises the emerging research issue of developing tools and models to predict the lifecycle inventory (LCI) and environmental impacts for different AM processes in the design stage.

One of the predominant material classes processed by AM are metals. A promising metal AM process is directed energy deposition (DED), which uses thermal energy, e. g., a laser beam, to melt metal powders or wires, e. g., stainless steel, aluminum alloys and titanium alloys, while they are deposited [4–6]. Reviewing the literature on the environmental aspects of DED, approaches to quantify the LCI of DED can be divided into three categories:

(i) Quantifications based on the white box principle, where details of a DED process are specified, and the calculation is based on mathematical equations between energy demand, power consumption, manufacturing time, material demand, and other parameters related to products or processes [7–9];

(ii) Quantifications based on the black box principle, where specific, but only total values related to material or energy demands are provided [3, 10–14];

(iii) Quantifications based on experiments, where material and energy demands are measured using experimental devices [15].

The approaches following the black box principle can only provide energy data for specific machines, on which the data were collected. These approaches can merely be transferred to different AM machines to a limited extent since different AM-machines have different system characteristics. Hence, transferring black box models to other AM-machine types requires additional effort in data collection. The approaches based on experiments

Fig. 1 Deposition principle of
HS DED-LB
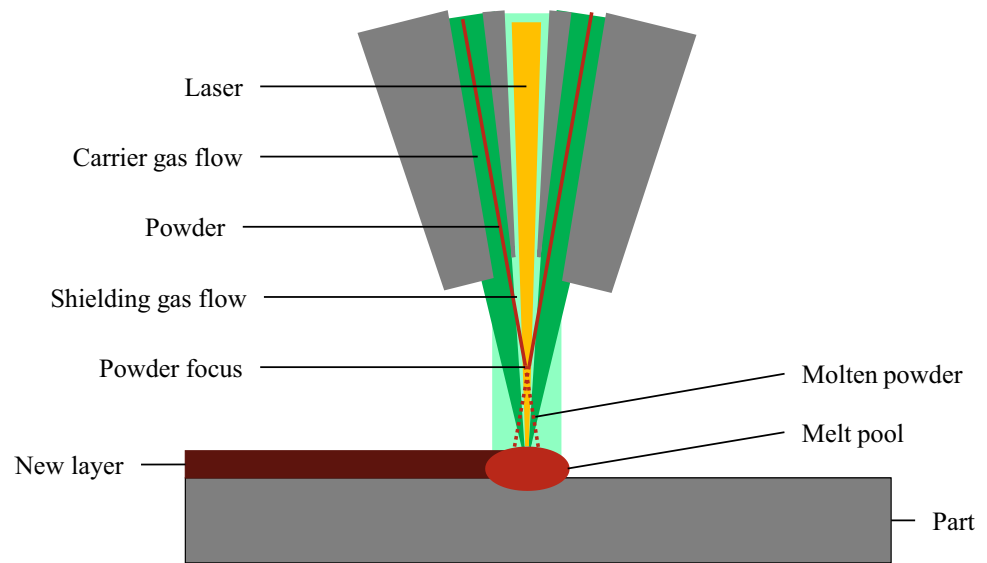
provide detailed and accurate energy information, but also require a significant effort and time for experimental setup. In addition, the results of these studies are specific to the investigated part and the corresponding process parameters, and therefore can only be transferred to other parts or process parameter settings to a limited extent. Only the approaches following the white box principle can provide a certain understanding of the interdependencies and system structure for a range of different AM-machines and can therefore be used to predict the energy demands to manufacture a part. A methodology called Unit Process Life Cycle Inventory (UPLCI) has been proposed by the research community to provide a convenient LCI calculation of various manufacturing processes following the white box principle. Thus, the UPLCI approach can be seen as a potential method for the LCI calculation of DED processes.

A UPLCI model describes the material and energy flows for a specific manufacturing process (denoted as a Unit Process), allowing the calculation of material and energy demands for accomplishing a manufacturing task using this process, without time- and cost-intense experiments [16]. So far, UPLCI models were developed for grinding, arc welding, and metal injection molding [17–19]. For AM, UPLCI models for stereolithography [20] and laser powder bed fusion [21] were developed in previous studies.

In the presented work, the research objective is to establish a reusable UPLCI model for DED. As the reference DED process, High-Speed Laser Directed Energy Deposition (HS DED-LB) is selected, where the powder focus is shifted about 10 mm above the build surface, as illustrated in Fig. 1. Hence, the powder is melted by the laser and applied in a liquid state [22]. This leads to very high process speeds compared to conventional DED. Therefore, HS DED-LB has a great potential for industrial application. However, the high process speeds result in a high power consumption, which is also highly varying due to the high variability of the process and the wide range of the adjustable process parameters, and therefore cannot be approximated by averaged values. Thus, this work focuses on the development of a UPLCI model for the HS DED-LB process, which will lead to benefits such as a more convenient assessment and improvement of the energy and environmental performance of HS DED-LB manufactured parts.

2 Methodology for unit process life cycle inventory model

To obtain a reusable model to predict the energy demand and material usage for HS DED-LB, the concept of "unit processes" is applied. The unit process consists of inputs, the manufacturing process, and outputs of an operation. Figure 2 shows the unit process of HS DED-LB, in which various forms of energy such as electrical energy are considered as input. The material inputs of the process are metal powder, inert gas such as argon, and if necessary, the substrate plate. Cooling water is circulated but may need to be refilled occasionally. The output of the process is a manufactured part (i.e., the product of the HS DED-LB process). The gaseous inputs, i.e., compressed air and inert gas, are released into the environment as emissions. Metal powder remaining after the build process are collected and can be screened and reused.

Fig. 2 Unit Process diagram of HS DED-LB
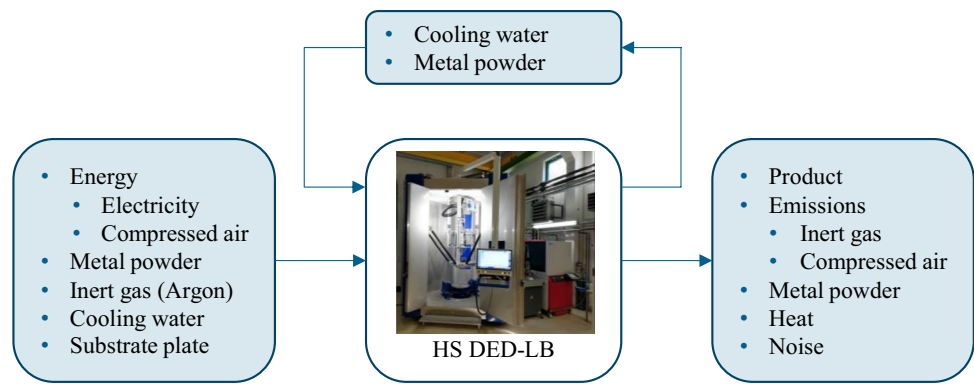
2.1 HS DED-LB process energy characteristics

In this work, the model is developed based on the reference HS DED-LB machine from the company Ponticon[1]. The HS DED-LB system has five subsystems that consume electricity independently. These subsystems include the trajectory system, the laser generator, the powder feeder, the suction system and other peripherical subsystems with the integrated cooling system. Thus, the total demand for electrical energy is the sum of the energy demands of the respective subsystems, as shown in Eq. 1.

$$E_{total} = E_{ts} + E_l + E_{pf} + E_e + E_s. \tag{1}$$

Figure 3 shows a sketch of a power curve of each subsystem during one build cycle. It can be divided into three phases: pre-step, in-step, and post-step [23]. In the following, the system characteristics and energy consumption mechanisms of the HS DED-LB process within each process step are described.

1. **Pre-step**

At the beginning of the build cycle, the inert gas flows are switched on, followed by a few seconds of waiting, until the inert gas flows have built up homogeneously. Afterwards, the powder feeder is switched on, which also takes a couple of seconds until the powder cone is complete and homogeneous. Both waiting times are defined individually as process parameters. During the pre-step, the laser generator and the trajectory system are in standby, and the suction system continues.

2. **In-step**

The in-step is the actual additive manufacturing process, where the material is deposited and therefore the part is manufactured during this period. The build platform is moved along the scan path defined in the G-Code at a speed, which is defined in the process parameters. Thereby the build platform is moved by the three motors of the trajectory system. The laser generator is switched on to enable the powder processing and deposition. Due to inertia, the trajectory systems require a certain traveling path before a change of direction to decelerate and re-accelerate to the required speed. Therefore, there are periods when the laser beam is not generated, but the laser generator is still ready to fire. Accordingly, all subsystems are switched on during the in-step. The duration of the in-step depends on the part geometry and the corresponding scan path as well as on the selected process parameters such as the trajectory speed.

3. **Post-step**

Immediately after the manufacturing process is finished, the laser generator and the powder feeder are switched back to standby. The build platform can optionally move at a slow speed to a previously defined position for a better part removal. The duration of the post-step comprises only a few seconds of waiting time, which are individually defined in the process parameters, but are necessary for the powder cone to decompose and for the build platform to stop so that the build chamber can be entered.

2.2 Parameters affecting the energy required for HS DED-LB

The energy demand of the HS DED-LB is influenced by several process parameters that are adjusted individually for each build cycle. The process parameters are ranked below from the greatest influence on energy demand to the least influence. However, the order is not absolute but rather indicates a tendency of the influence strength based on Ehmsen et al. [23]. An absolute and standardized order cannot be

---

[1] Naming of specific manufacturers is done solely for the sake of completeness and does not necessarily imply an endorsement of the named companies nor that the products are necessarily the best for the purpose.
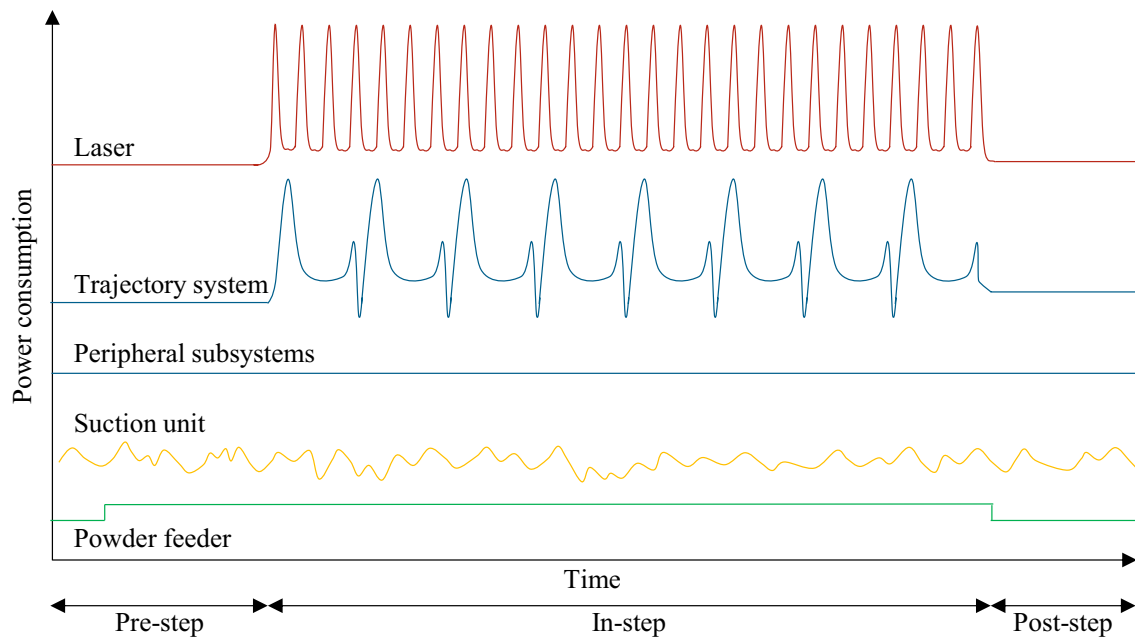
Fig. 3 Illustration of power curves of the individual subsystems during a build cycle (the level of power consumption is only qualitative)

created since the strength of the influence depends on the respective configuration.

For electrical energy:

1. Laser power,
2. Trajectory speed,
3. Geometry of the part and the scan path based on it,
4. Extraction rate of the suction,
5. Speed of the stirrer in the powder container,
6. Speed of the powder conveyor disc.

For powder:

7. Powder mass flow.

For inert gas:

8. Shielding gas flow,
9. Carrier gas flow.

For coolant:

10. Coolant refill amount,
11. Coolant refill intervals.

For modeling the UPLCI, all listed parameters as well as their influence on the energy consuming behavior of the subsystems are described below.

2.2.1 Build cycle time

The energy demand is the time integral of power, and therefore, before the energy demand of HS DED-LB is modeled, the time information should be clarified at first. Since this work considers the HS DED-LB process in three phases, the total process time t_{total} can be regarded as the sum of the times for each phase, as shown in Eq. 2.

$$t_{total} = t_{pre} + t_{in} + t_{post}. \tag{2}$$

The duration time of the pre-step t_{pre} and the post-step t_{post} are set as process parameters and are known by users prior to the start of a build cycle. In contrast, the time for the in-step t_{in} is not given by users and manifests individually for each build cycle. Hence, t_{in} must be described by the parameters related to the build process. In this work, t_{in} is approximated based on the movement of the trajectory system since this duration depends on the selected scan path and the trajectory speed. In particular t_{in} is composed of the following elements in Eq. 3:

$$t_{in} = t_{track} + t_{ac} + t_{deac} + 2 \cdot t_{remaining} + t_{switch}. \tag{3}$$

- time to travel along the part geometry at the required speed t_{track} (Eq. 4): This is usually equal to the time the laser is on $t_{l,on}$ whereby material is deposited. t_{track} can thus be determined by the number of layers N_{layer} and the length of the scan path per layer at which material

is deposited l_{layer}. The resulting total distance is divided by the feed rate v_{ts}.

$$t_{track} = t_{l,on} = \frac{l_{layer} \cdot N_{layer}}{v_{ts}}. \tag{4}$$

- time until the required speed is reached t_{ac} (Eq. 5): Depending on the scan path there are distances for accelerating and decelerating the build platform to the required speed. To check whether a scan path has at least one turning point, the binary variable B is 1, if there are no turning points, B is set to 0. If there are turning points, the scan path has several paths per layer, whose number is expressed in $N_{path\,per\,layer}$. By multiplying this with the number of layers N_{layer} and the time to reach the required speed (h) $t_{ac,path}$ the total time within a process cycle for accelerating the build platform t_{ac} can be determined.

$$t_{ac} = t_{ac,path} \cdot N_{path\,per\,layer} \cdot N_{layer} \cdot B. \tag{5}$$

- time to decelerate before the turning point t_{deac} (Eq. 6): As already described for t_{ac}, t_{deac} is calculated analogously by the product of the time to reduce the speed to change direction $t_{deac,path}$, the number of paths per layer $N_{path\,per\,layer}$, the number of layers N_{layer} and the binary variable B.

$$t_{deac} = t_{deac,path} \cdot N_{path\,per\,layer} \cdot N_{layers} \cdot B. \tag{6}$$

- time to travel the remaining acceleration distance and deceleration distance at reached speed $t_{remaining}$ (Eq. 7): Normally, a safety distance between the acceleration distance and the actual scan path is included in the G-code. Here the build platform travel at the set speed, but no material is applied yet. First, the remaining distance must be calculated. For this purpose, the actual acceleration distance, which can be calculated by the basic relationship between acceleration a and time to reach the required speed $t_{ac,path}$, is subtracted from the scan path length to accelerate and decelerate $l_{ac/deac}$, defined in the process parameters. The time needed to travel this distance is then divided by the speed v_{ts} and multiplied by the number of layers N_{layer} and the number of paths per layer $N_{path\,per\,layer}$. Again, a binary variable B is used to check whether turning points and thus remaining acceleration distances exist.

$$t_{remaining} = N_{path\,per\,layer} \cdot N_{layer} \frac{l_{ac/deac} - \frac{1}{2} \cdot a \cdot t_{ac,path}^2}{v_{ts}} \cdot B. \tag{7}$$

- time to switch layers t_{switch} (Eq. 8): To calculate the time which is necessary to switch layers within a build cycle the time for switching from one layer to another $t_{switch\,per\,layer}$ and the number of layers N_{layer} are multiplied.

$$t_{switch} = t_{switchperlayer} \cdot N_{layer}. \tag{8}$$

2.2.2 Energy requirement of the peripheral subsystems

In general, the energy demand can be determined by the relation of the required power and the time. The power consumption of the peripheral subsystems run continuously during the entire build cycle. Therefore, the energy demand of the peripheral subsystems E_s (in Wh) can be determined by multiplying the required power of the peripheral subsystems P_s (in W) and the time needed for completing one build cycle t_{total} (in h), as shown in Eq. 9.

$$E_s = P_s \cdot t_{total}. \tag{9}$$

2.2.3 Energy requirement of the laser generator

Depending on the geometry of the part, the laser is not continuously scanning during the in-step but is rather switched on and off as needed. Therefore, the energy demand of the laser generator E_l (in Wh) is composed of three energy demands, as shown in Eq. 10, which must be differentiated:

- Energy consumption of the laser generator while it is switched on and melts powder to deposit, $E_{l,on}$ (in Wh),
- Energy consumption of the laser generator while it is ready to fire between each laser pulse, $E_{l,ready}$ (in Wh),
- Energy consumption of the laser generator while standby during the pre-step and post-step, $E_{l,standby}$ (in Wh).

$$E_l = E_{l,on} + E_{l,ready} + E_{l,standby}. \tag{10}$$

The energy demand of the laser generator during standby $E_{l,standby}$ can be calculated based on power and time (Eq. 11). Since the laser generator is in standby only during the pre-step and post-step, the required time is the sum of those two process parameters t_{pre} and t_{post} (both in h). The required power $P_{l,standby}$ (in W) is independent from any process parameter and can be assumed to be constant. $P_{l,standby}$ must be determined individually for the considered system.

$$E_{l,standby} = P_{l,standby} \cdot \left(t_{pre} + t_{post}\right). \tag{11}$$

Analogously, the calculation of the energy demand for the period, during which the laser generator is ready to fire, is the product of the required power and the corresponding time. Similar to the power consumption during standby, the power consumption while the laser is ready to fire $P_{l,ready}$ (in W) is independent of the set laser power and can be assumed to be constant. The time can easily be calculated

by subtracting the time for the in-step t_{in} and the time during which the laser is on $t_{l,on}$ (see Eq. 17) (both in h), as shown in Eq. 12.

$$E_{l,ready} = P_{l,ready} \cdot \left(t_{in} - t_{l,on} \right). \quad (12)$$

To calculate the energy demand of the laser during operating $E_{l,on}$ (in Wh), both the power consumption $P_{l,on}$ (in W) and the corresponding time $t_{l,on}$ (in h) must be determined and can then be calculated as shown in Eq. 13.

$$E_{l,on} = P_{l,on} \cdot t_{l,on}. \quad (13)$$

The required power consumption of the laser $P_{l,on}$ (in W) depends on the set laser power $P_{l,set}$ (in W). In general, the required power increases with a higher laser power setting. In Ehmsen et al. it was found that there is a linear relationship between the required power and the set laser power [23]. Thus, the required power can be described by a linear function. For this, $P_{l,ready}$ serves as the y intercept. The proportionality factor for the slope is the difference between the required power at the maximum set laser power $P_{l,max}$ (in W) and the required power during the mode ready to fire $P_{l,ready}$. By inserting the set laser power $P_{l,set}$ as share of the maximum set laser power $P_{l,set,max}$ (both in W), the required power can now be calculated with Eq. 14.

$$P_{l,on} = P_{l,ready} + \left(\left(P_{l,max} - P_{l,ready} \right) \cdot \frac{P_{l,set}}{P_{l,set,max}} \right). \quad (14)$$

The maximum required power $P_{l,max}$ can be determined in three different ways. Firstly, it can be determined experimentally, secondly, it can be found in the specification of the laser generator, and thirdly, it can be calculated based on the efficiency of the laser η_l (in percent) as described in Eq. 15.

$$P_{l,max} = \frac{P_{l,set,max}}{\eta_l}. \quad (15)$$

The time the laser is switched on $t_{l,on}$ (h) can be determined based on the scan path length l_{layer} (in m) traversing the part geometry for each layer N_{layer} (in amount) and the trajectory speed v_{ts} (in m/h) (Eq. 16).

$$t_{l,on} = \frac{l_{layer} \cdot N_{layer}}{v_{ts}}. \quad (16)$$

2.2.4 Energy requirement of the powder feeder

The powder feeder runs continuously during pre-step and in-step and is set to standby in post-step. Therefore, the total energy demand of the powder feeder E_{pf} (Wh) is the sum of the energy demand when the powder feeder is operating $E_{pf,on}$ (in Wh) and when it is on standby $E_{pf,standby}$ (in Wh), see Eq. 17.

$$E_{pf} = E_{pf,on} + E_{pf,standby}. \quad (17)$$

The energy demand when the powder feeder is operating $E_{pf,on}$ (in Wh) can be calculated by the required power $P_{pf,on}$ (in W) over the respective time of the pre-step t_{pre} and in-step t_{in} (both in h) (Eq. 18).

$$E_{pf,on} = P_{pf,on} \cdot \left(t_{pre} + t_{in} \right). \quad (18)$$

The stirrer speed $v_{pf,s,set}$ and the conveyor disc speed $v_{pf,c,set}$ (both in s^{-1}) are influencing the energy demand of the powder feeder independently from each other [23]. Subsequently, the power consumption must be divided into three parts. $P_{pf,on,b}$ (in W) is the base power during operation, which is independent of the two process parameters. Therefore, it is constant and must be determined through experiments. $P_{pf,on,s}$ (in W) is the power component, which depends on the stirrer speed, and $P_{pf,on,c}$ (in W) is the power component, which depends on the conveyor disc speed. The consumed power $P_{pf,on}$ is therefore the sum of those three power consumptions, as shown in Eq. 19.

$$P_{pf,on} = P_{pf,on,s} + P_{pf,on,c} + P_{pf,on,b}. \quad (19)$$

There is a linear increase in the required power at higher speeds for both process parameters [23]. Therefore, the required power for each process parameter can be calculated using the same principle as for $P_{l,on}$. Starting from the respective base powers $P_{p,on,s,b}$ and $P_{pf,on,c,b}$ (both in W) which serve as the y-intercept, the proportionality factor is calculated by the difference between the maximal required power $P_{pf,on,s,max}$ and $P_{pf,on,c,max}$ (both in W) and the respective base power (Eqs. 20 and 21). The maximal required power as well as the base power must be determined experimentally for both, the stirrer, and the conveyor disc. To determine the x-intercept, the relative speed of the stirrer and the conveyor disc can be calculated by the quotient of the set stirrer speed $v_{pf,s,set}$ or set conveyor disc speed $v_{pf,c,set}$ (both in s^{-1}) and the respective maximum possible set speed of the stirrer $v_{pf,s,set,max}$ or set conveyor disc speed $v_{pf,c,set,max}$ (both in s^{-1}).

$$P_{pf,on,s} = P_{pf,on,s,b} + \left(P_{pf,on,s,max} - P_{pf,on,s,b} \right) \cdot \frac{v_{pf,s,set}}{v_{pf,s,set,max}}. \quad (20)$$

$$P_{pf,on,c} = P_{pf,on,c,b} + \left(P_{pf,on,c,max} - P_{pf,on,c,b} \right) \cdot \frac{v_{pf,c,set}}{v_{pf,c,set,max}}. \quad (21)$$

The energy requirement of the powder feeder during standby $E_{pf,standby}$ (in Wh) is the product of the set post-step time t_{post} and the required power during standby $P_{pf,standby}$ (in W) (Eq. 22). The required power during standby must be determined experimentally and is constant as well as independent of other process parameters.

$$E_{pf,standby} = P_{pf,standby} \cdot t_{post}. \tag{22}$$

2.2.5 Energy requirement of the suction

The suction system runs continuously through the entire build cycle. Thus, the energy demand E_e (in Wh) equals to the power consumed P_e (in W) over the entire time of the build cycle t_{total} (Eq. 23).

$$E_e = P_e \cdot t_{total}. \tag{23}$$

Previous analyses of the suction system show a strongly fluctuating power consumption during stationary operation [23]. Nevertheless, the power consumption of the suction system can be approximated by an average power. The previous experiments also showed for our investigated suction system, that a case distinction is necessary to estimate the power consumption. Below a relative extraction rate of 36%, the power consumption is constant and corresponds to the power consumption during standby $P_{e,b}$, (in W) which must be determined experimentally. Above an relative extraction rate of 36%, the required power increases disproportionately and can be approximated by a quadratic function [23]. To obtain this, another parameter is required in addition to the required basic power and the maximum power. In order to obtain a function with comparatively low complexity using the Gaussian elimination method with unknown points, three points must be defined. As before, the power consumption at the minimum and the maximum set extraction rate are chosen as significant points, which corresponds to $\left(0|P_{e,b}\right)$ and $\left(1|P_{e,max}\right)$. In addition to this, to obtain a quadratic function, an additional power consumption at a relative extraction rate of 50%, i. e. the set extraction volume $\dot{V}_{e,set}$ (in m³/h) corresponds to half of the maximum possible extraction volume $\dot{V}_{e,set,max}$ (in m³/h), was added as significant point, therefore $\left(0.5|P_{e,50\%}\right)$ applies. This was chosen because, the extraction rate of 50% lies exactly between the other two selected extraction rates, ensuring that the resulting function corresponds to the total range of adjustable extraction volumes. By performing the Gaussian elimination, Eq. 25 can be obtained. However, the critical value of 36% may vary for different suction systems and may need to be adjusted individually.

2.2.6 Energy requirement of the trajectory system

The trajectory system moves the build platform along the defined scan path. The energy demand of the trajectory system E_{ts} (in Wh) also consists of two components, when the build platform is moving $E_{ts,on}$ and when it is in standby $E_{ts,standby}$ (both in Wh) (Eq. 25).

$$E_{ts} = E_{ts,on} + E_{ts,standby}. \tag{25}$$

During the pre-step and the post-step, the trajectory system is in standby. Thus, the energy demand $E_{ts,standby}$ can be calculated based on the respective consumed power over time $P_{ts,standby}$ (in W), as shown in Eq. 26. The power consumption here is constant and must be determined experimentally.

$$E_{ts,standby} = P_{ts,standby} \cdot \left(t_{pre} + t_{post}\right). \tag{26}$$

The power consumption during the in-step is primarily dependent on the trajectory speed v_{ts} (in m/h), but different scan paths also result in different power consumption curves. Thus, a case distinction between a rather linear scan path with turning points and a rather rotationally symmetric scan path without turning points is necessary, as shown in Eq. 27.

$$E_{ts,on} = \begin{cases} Eq.(28), & if\ scanpath = rotational \\ Eq.(30), & if\ scanpath = linear \end{cases}. \tag{27}$$

The energy demand, when the scan path is rotationally symmetric $E_{ts,on,circle}$ (in Wh), is calculated by multiplying the respective power consumption $P_{ts,on,circle}$ (in W) with the time for the in-step t_{in}, as shown in Eq. 28.

$$E_{ts,on,circle} = P_{ts,on,circle} \cdot t_{in}. \tag{28}$$

When analyzing rotationally symmetric scan paths, it was noticed that the power consumption of the trajectory system increases disproportionately as the speed v_{ts} (in m/s) increases [23]. Thus, the equation is derived using the Gaussian elimination, based on the power consumption during standby $P_{ts,standby}$, the power consumption during travelling a circle at maximum speed $P_{ts,circle,max}$, and at a speed which corresponds to 50% of the maximum possible

$$P_e = \begin{cases} P_{e,b}, & if\ \frac{\dot{V}_{e,set}}{\dot{V}_{e,set,max}} < 36\% \\ \left(2P_{e,max} - 4P_{e,50\%} + 2P_{e,b}\right)\left(\frac{\dot{V}_{e,set}}{\dot{V}_{e,set,max}}\right)^2 + \left(-P_{e,max} + 4P_{e,50\%} - 3P_{e,b}\right) \cdot \frac{\dot{V}_{e,set}}{\dot{V}_{e,setmax}} \\ + P_{e,b}, & if\ \frac{\dot{V}_{e,set}}{\dot{V}_{e,set,max}} \geq 36\%. \end{cases} \tag{24}$$

speed $v_{ts,max}$ (in m/s), $P_{ts,circle,\ 50\%}$ (all in W). However, a third-grade function is required for a suitable description. Therefore, a fourth point, here the required power at a speed of 75% of the maximum speed, $P_{ts,circle,\ 75\%}$ (in W) is added. The result of the Gaussian elimination is given in Eq. 29.

$$
\begin{aligned}
P_{ts,on,linear,ac} \\
= \left(P_{ts,linear,ac,max} - P_{ts,linear,ac,min}\right) \cdot \\
\frac{v_{ts}}{v_{ts,max}} + P_{ts,linear,ac,min},
\end{aligned}
\tag{32}
$$

$$
\begin{aligned}
P_{ts,on,circle} &= \left(8P_{ts,circle,max} - 21.33P_{ts,circle,75\%} + 16P_{ts,circle,50\%} - 2.67P_{ts,standby}\right) \cdot \left(\frac{v_{ts}}{v_{ts,max}}\right)^3 \\
&+ \left(-10P_{ts,circle,max} + 32P_{ts,,circle,75\%} - 28P_{ts,circle,50\%} + 6P_{ts,standby}\right) \cdot \left(\frac{v_{ts}}{v_{ts,max}}\right)^2 \\
&+ \left(3P_{ts,circle,max} - 10.67P_{ts,circle,75\%} + 12P_{ts,circle,50\%} - 4.33P_{ts,standby}\right) \cdot \frac{v_{ts}}{v_{ts,max}} \\
&+ P_{ts,standby}.\#
\end{aligned}
\tag{29}
$$

The power consumption of a rather linear scan path can be distinguished between the power consumption of acceleration $P_{ts,on,linear,ac}$, the power consumption for keeping the speed $P_{ts,on,linear,path}$ and the power consumption for deceleration before the turning point $P_{ts,on,linear,deac}$ (all in W) [23]. This pattern is repeated for each scan path. Thus, each power consumption must be multiplied with the corresponding time periods for acceleration $t_{ts,on,linear,ac}$, for deceleration $t_{ts,on,linear,deac}$ (both in h) and the remaining time of the in-step in which the speed is maintained, to obtain the energy demand, as shown in Eq. 30.

$$
\begin{aligned}
cE_{ts,on,linear} = P_{ts,on,linear,path} \cdot \big(t_{in} - t_{ts,on,linear,ac} \\
- t_{ts,on,linear,deac}\big) + P_{ts,on,linear,ac} \cdot t_{ts,on,linear,ac} \\
+ P_{ts,on,linear,deac} \cdot t_{ts,on,linear,deac}.
\end{aligned}
\tag{30}
$$

The consumed power increases linearly with an increase in speed for accelerating $P_{ts,on,linear,ac}$, decelerating $P_{ts,on,linear,deac}$, and for maintaining the speed $P_{ts,on,linear,path}$ (all in W). Therefore, the power consumed can be linearly extrapolated, as shown in Eqs. 31, 32 and 33. For this, as with linear functions before, the y-axis intercept is defined by the respective minimum power consumption $P_{tslinear,path,min}$, $P_{ts,linear,ac,min}$, and $P_{ts,linear,deac,min}$ (all in W) and the respective maximum power consumption $P_{ts,linear,path,max}$, $P_{ts,linear,ac,max}$, and $P_{ts,linear,deac,max}$ (all in W). The slope is again defined by the difference between the maximum power consumption and the minimum power consumption.

$$
\begin{aligned}
P_{ts,on,linear,path} \\
= \left(P_{ts,linear,path,max} - P_{ts,linear,path,min}\right) \cdot \\
\frac{v_{ts}}{v_{ts,max}} + P_{ts,linear,path,min},
\end{aligned}
\tag{31}
$$

$$
\begin{aligned}
P_{ts,on,linear,deac} \\
= \left(P_{ts,max,linear,deac} - P_{ts,min,linear,deac}\right) \cdot \\
\frac{v_{ts}}{v_{ts,max}} + P_{ts,min,linear,deac}.
\end{aligned}
\tag{33}
$$

The time for acceleration $t_{ts,on,linear,ac}$ and deceleration $t_{ts,on,linear,deac}$ (both in h) is also dependent on the speed to be reached v_{ts} (in m/h) and can be described linearly, in the same mathematical structure, as shown in Eqs. 34 and 35.

$$
\begin{aligned}
t_{ts,on,linear,ac} \\
= \left(t_{ts,linear,ac,max} - t_{ts,linear,ac,min}\right) \cdot \frac{v_{ts}}{v_{ts,max}} + t_{ts,linear,ac,min},
\end{aligned}
\tag{34}
$$

$$
\begin{aligned}
t_{ts,on,linear,deac} \\
= \left(t_{ts,linear,deac,max} - t_{ts,linear,deac,min}\right) \cdot \\
\frac{v_{ts}}{v_{ts,max}} + t_{ts,linear,deac,min}.
\end{aligned}
\tag{35}
$$

2.2.7 Summary on unit process life cycle energy

If the following variables in Table 1 are collected experimentally, the energy demand can be estimated by entering the process parameters defined for the build cycle.

2.3 HS DED-LB process material characteristics

In our UPLCI model, only the powder materials and inert gas are considered. The compressed air is required to clean the filters of the suction system, which usually takes place at the end of a workday. Furthermore, compressed air is required for decelerating the build platform, as well as smaller consumptions, e.g. when changing the powder during the process. Moreover, cooling water is only refilled

Table 1 Overview of the variables to be determined to apply the model

Subsystems	Laser	Powder feeder	Suction	Trajectory system		
				General	Rotational scan path	Linear scan path
P_s	η_l	$P_{pf,on,b}$	$P_{e,b}$	a	$P_{ts,circle,max}$	$P_{ts,linear,ac,max}$
	$P_{l,max}$	$P_{pf,on,c,b}$	$P_{e,max}$	$l_{ac/deac}$	$P_{ts,circle,50\%}$	$P_{ts,linear,deac,max}$
	$P_{l,ready}$	$P_{pf,on,c,max}$	$P_{e,50\%}$	$P_{ts,standby}$	$P_{ts,circle,75\%}$	$P_{ts,linear,path,max}$
	$P_{l,standby}$	$P_{pf,on,s,b}$		$t_{deac,path}$		$P_{ts,linear,ac,min}$
		$P_{pf,on,s,max}$		$t_{ac,path}$		$P_{ts,linear,deac,min}$
		$P_{pf,standby}$		$t_{switch\ per\ layer}$		$P_{ts,linear,path,min}$
						$P_{ts,standby}$
						$t_{ts,on,linear,ac}$
						$t_{ts,on,linear,deac}$
						$t_{ts,linear,ac,max}$
						$t_{ts,linear,deac,max}$
						$t_{ts,linear,ac,min}$
						$t_{ts,linear,deac,min}$

when required. If the consumption of the water and compressed air is allocated to the parts, the consumption per part is not significant so that these two consumables can be neglected in the UPCLI model.

2.3.1 Quantifying powder requirement

The powder feeder is switched on at the beginning of the pre-step and switched off immediately after completion of the in-step. How much powder is conveyed can be extrapolated over the process time to determine the total powder requirement m_{powder} (in g) for the process as shown in Eq. 36. The powder mass flow $\dot{m}$ (in g per h) is defined by the rotational speed of the conveyor disc $v_{pf,c,set}$ (in s^{-1}) and is individual for each material and can also vary between different charges of the same material. Therefore, the powder mass flow resulting from the rotational speed of the conveyor disc must be determined individually before the start of the process. This can be achieved by extrapolating the conveyed powder masses according to a stepwise increase in the rotational speed of the conveyor disc. Alternatively, the powder mass flow can also be calculated by the rotational speed of the conveyor disc and the volume of the channel in the conveyor disc, which is calculated by the product of Cross-sectional area Q_c (in m^2) and the Circumference of the channel u_c (in m), and the density of the powder ρ_{powder} (in g/m^3), according to Eq. 37.

$$m_{powder} = \dot{m} \cdot \left(t_{pre} + t_{in} \right), \tag{36}$$

$$\dot{m} = 3600 \cdot v_{pf,c,set} \cdot u_c \cdot Q_c \cdot \rho_{powder}. \tag{37}$$

However, only a small share of the powder conveyed is applied. The powder losses m_{loss} (in g) can be calculated according to Eq. 38. Schaible et al. classifies two types of powder losses. Machine-related powder losses $m_{loss,machine}$ (in g) occurs due to the necessary acceleration and deceleration distances for the build platform, where the laser is off, but the powder is still being conveyed. Thus, this type of powder loss can be calculated by Eq. 39 by determining the mass of the conveyed powder during the laser is turned off. Process-related powder losses $m_{loss,process}$ (in g), are caused by process physical effects such as evaporation of particles and overspray. They occur only while the laser is on [22]. Therefore, for calculation, the mass of the manufactured part m_{part} (in g) is subtracted from the powder mass flow $\dot{m}$ (in g per h) during the laser is turned on $t_{l,on}$ (in h).

$$m_{loss} = m_{loss,machine} + m_{loss,process}, \tag{38}$$

$$m_{loss,machine} = \dot{m} \cdot \left(t_{pre} + t_{in} - t_{l,on} \right), \tag{39}$$

$$m_{loss,process} = \dot{m} \cdot t_{l,on} - m_{part}. \tag{40}$$

2.3.2 Quantifying inert gas requirement

There are two inert gas flows. Therefore, the total inert gas demand V_i (in l) is the sum of both flows, as shown in Eq. 41. The carrier gas flow $\dot{v}_{i,c}$ (in l/h), transports the powder from the conveyor disc to the nozzle. The shielding gas flow $\dot{v}_{i,s}$ (in l/h), which passes through the inside of the laser optics, protects it from contamination. Both gas flow rates are defined in the process parameters. Thus, the needed volumes $V_{i,c}$ and $V_{i,s}$ (both in l) can be extrapolated over time, as shown in Eq. 42 for the carrier gas flow and in Eq. 43 for the shielding gas flow.

Table 2 Experimentally determined variables

$t_{ac,path}$	s	0.0504	$P_{ts,circle,max}$	W	19,741.2	$P_{ts,linear,deac,min}$	W	1986.5
$t_{deac,path}$	s	0.0504	$P_{ts,standby}$	W	1250.3	$P_{e,b}$	W	402.6
a	m/s^2	10.0	$P_{ts,linear,path,max}$	W	4168.0	$P_{e,50\%}$	W	757.4
t_{switch}	s	0.054	$t_{ts,linear,ac,max}$	s	0.1464*	$P_{e,max}$	W	4007.8
$P_{l,standby}$	W	2343.4	$t_{ts,linear,ac,min}$	s	0.0748	$P_{pf,s,b}$	W	23.3
$P_{l,ready}$	W	4368.4	$t_{ts,linear,deac,max}$	s	0.1425*	$P_{pf,s,max}$	W	30.4
$P_{l,max}$	W	26,652.9	$t_{ts,linear,deac,min}$	s	0.0583	$P_{pf,c,b}$	W	1.3
$P_{l,standby}$	W	2020.6	$P_{ts,linear,ac,max}$	W	19,289.4*	$P_{pf,c,max}$	W	10.1
$P_{ts,circle,50\%}$	W	8622.2	$P_{ts,linear,ac,min}$	W	1282.2	$P_{pf,standby}$	W	92.7
$P_{ts,circle,75\%}$	W	4237.4	$t_{ts,linear,deac,max}$	W	7271.5	$v_{ts,max}$	m/s	3.33

* Extrapolated based on measurements

$$V_i = V_{i,c} + V_{i,s}, \tag{41}$$

$$V_{i,c} = \dot{v}_{i,c} \cdot \left(t_{pre} + t_{in} \right), \tag{42}$$

$$V_{i,s} = \dot{v}_{i,s} \cdot \left(t_{pre} + t_{in} \right). \tag{43}$$

3 UPLCI model validation

For validation, the measured energy demand and the time of the build cycle was compared with the energy demand calculated by the model.

3.1 Experimental setup

The model from chapter 2 was validated on the reference HS DED-LB system (Ponticon pE3D). To generate the laser beam, the LDF 8000-6 diode laser by Laserline was used, which offers a laser power between 504 and 8400 W. The powder is stored in a container on the Twin-150-ARN216-OP by Oerlikon Metco. The stirrer speed can be up to 55 s^{-1} and the conveyor disc speed between 0.003 and 0.167 s^{-1}. Unapplied powder is extracted by the Dustomat 4–24 W3 eco + dry extractor by ESTA, which has an extracted volume per hour between 770 and 2540 m^3/h. The consumed power was measured with

several appropriately dimensioned current transformers and a corresponding EtherCAT terminal by Beckhoff, which shows the recorded power per millisecond for the entire AM system as well as individually for the laser generator, the powder feeder, and the suction system. Thus, the energy demand of the trajectory system and the subsystem can only be determined jointly. In contrast to the suction system, the powder feeder and the laser generator, the trajectory system is not an independent subsystem. Its three motors are located at three different places in the pE3D system. The control equipment of the trajectory system is located centrally in the control cabinet together with the peripheral subsystems, such as the central control unit. Individual measurement of the trajectory system is therefore only possible with great effort. Since the peripheral subsystems have a constant power consumption, the power consumption caused by the trajectory system can still be measured, analyzed, and modeled individually.

The relevant variables were determined in corresponding experiments and are listed in Table 2. The power and time data listed here, were obtained using the described experimental set up. For statistical validity, each experiment was performed at least three times and the respective mean value was calculated and applied. Theoretic data, such as minimum power inputs, were extrapolated from the measurement results. An analysis of the influence of the process parameters and individual subsystems can be found in Ehmsen et al. [23].

Fig. 4 Validation parts

| Cuboid | Logo | Cylinder |

Table 3 Overview of process parameters for parts for validation

Process iarameter	Unit	Part 1: Cuboid	Part 2: Logo	Part 3: Cylinder
Dimension (l×w×h)	m	$0.015\times0.081\times0.005$	$0.077\times0.038\times0.003$	Ø 0.12×0.0167
v_{ts}	m/s	1.33	0.17	0.33
$P_{l,set}$	W	3200	1380	600
$v_{pf,c,set}$	s^{-1}	0.092	0.093	0.55
$v_{pf,s,set}$	s^{-1}	16.5	16.5	16.5
$\dot{V}_{e,set}$	m^3/s	0.47	0.47	0.47
N_{layer}	–	80	5	200
$N_{path\ per\ layer}$	–	8	63	1
l_{layer}	m	0.12	4.926	0.377
$l_{ac/deac}$	m	0.1	0.05	–
t_{pre}	s	23	15	18
t_{post}	s	10	10	10

As material, gas atomized 316L stainless steel (EN 1.4404) produced by Oerlikon metco with a nominal particle size distribution of 45 μm + 15 μm was used. Three parts, a cuboid, a logo, and a hollow cylinder, which can be seen in Fig. 4 were manufactured. The dimensions of the parts and the respective process parameters can be found in Table 3.

3.2 Energy model validation

During the manufacturing of the parts, the consumed power was measured for the laser, the powder feeder, the suction, and for the total system. The power curve for the cuboid is
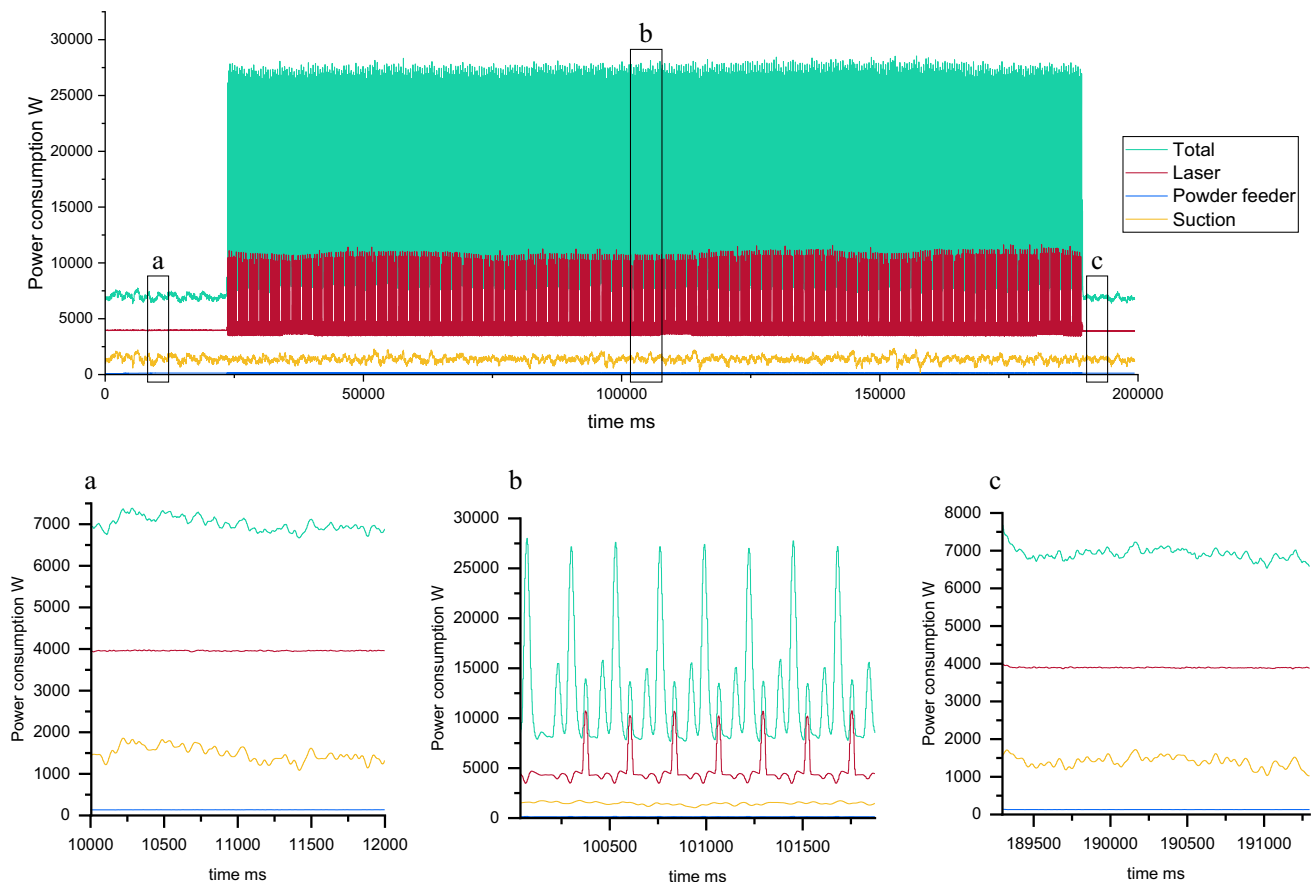
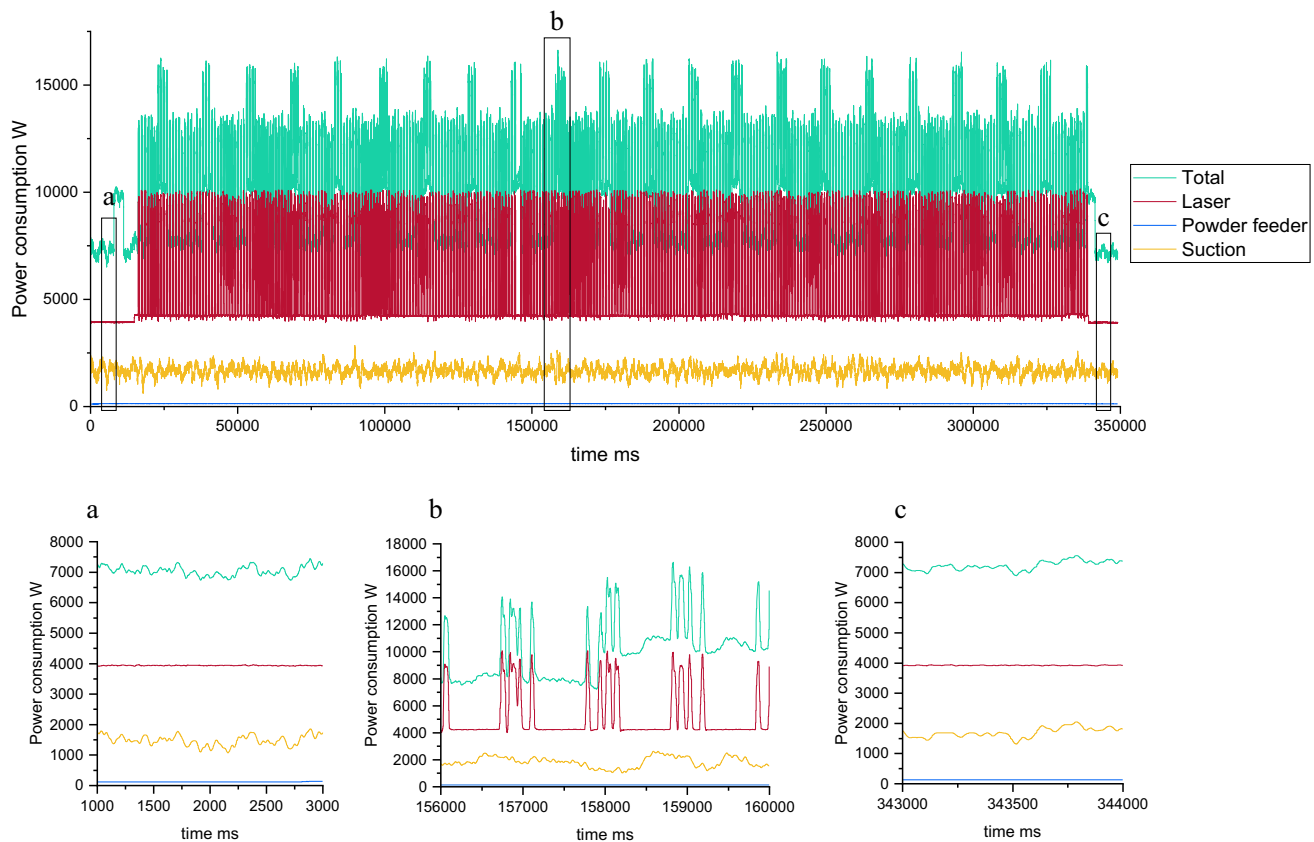**Fig. 5** Power curve of the of the cuboid

Fig. 6 Power curve of the logo

shown in Fig. 5, for the logo in Fig. 6 and for the cylinder in Fig. 7.

The energy demand calculated from the respective power measurements was then compared with the values calculated from the UPLCI model. For the cuboid, a deviation of 3% was observed. For the logo, the calculated energy demand was 2% higher than the measured value. Finally, the calculated energy demand of the cylinder deviates only by 1% from the measured energy demand, which can be seen in Table 4. However, the energy demand of individual subsystems, such as the suction and the trajectory system in particular, deviate from their measured values. The suction was set to the same extracted volume for all three trials, but the energy demand predicted by the model is too high for the cuboid and the logo with a deviation of 12%, and 2% respectively, and once too low for the cylinder with a deviation of 5%. This can be explained by the highly fluctuating power consumption of the suction unit, which has irregular power fluctuations of up to 2000 W. In the case of the cylinder, a large deviation in the model results for the trajectory system. There is a very high variability in the choice of scan path and each scan path results in a different power consumption curve. Thus, although the geometry

remains the same, a different circumference can already lead to a change in power consumption, since the three motors for the build platform must accelerate and decelerate more quickly to complete a smaller circumference than a large one. For all three parts, the cycle time was modeled as too long, which in turn has an increasing effect on the modeled energy demand. The use cases show that the determination of the time of the build cycles can cause deviations. Therefore, it should be aimed that the build cycle time is modeled more precisely, for example within an automatically generated G-code. These modeled times can be used in the UPLCI model instead. For the use case of the logo, it was assumed that the laser is switched on only half of the length of each layer l_{layer}. Therefore, the factor $t_{l,on}$ was multiplied by 0.5.

4 Conclusions

This paper presents the reusable calculation model based on the UPLCI method to analyze the environmental impact of HS DED-LB. With the developed model, the energy demand and material requirements of different parts manufactured
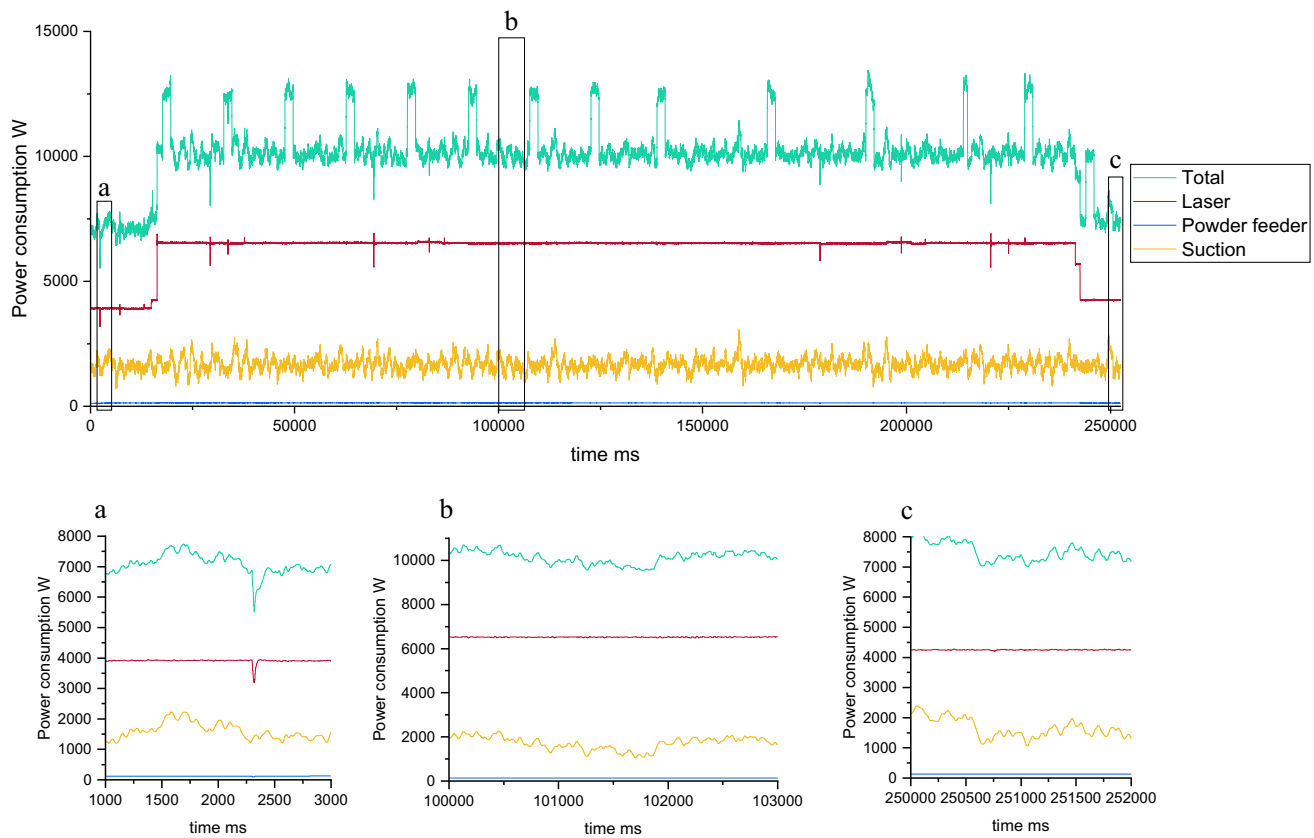
Fig. 7 Power curve of the cylinder

Table 4 Results of the experiments and comparison with the estimated energy demand of the presented model

Energy demand	Part 1: Cuboid			Part 2: Logo			Part 3: Hollow cylinder		
	Experiment	Model	Deviation (%)	Experiment	Model	Deviation (%)	Experiment	Model	Deviation (%)
E_{total} (Wh)	629.56	608.81	−3	901.72	917.97	2	705.62	713.82	1
E_l (Wh)	257.93	241.43	−6	510.58	510.27	0	439.47	405.58	−8
E_{pf} (Wh)	7.56	7.06	−7	13.36	13.55	1	9.44	8.91	−6
E_e (Wh)	77.32	86.93	12	162.26	165.81	2	117.60	111.21	−5
E_{ts} (Wh)	286.75	273.39	−5	215.52	228.33	6	139.10	188.12	35
t_{total} (s)	199.34	207.00	4	349.07	394.82	13	252.41	264.80	5

by DED-LB can be evaluated in a simplified way. To adapt the model individually to different AM systems, power consumption of the individual subsystems, e.g., during standby, must be determined experimentally. Maximum power consumptions can either be determined experimentally as well or can be obtained from machine specifications of the individual subsystems. Based on the experiments and results, the following conclusions were confirmed. First, the power consumption of each subsystem is influenced by different process parameters. Especially the choice of the scan path has an impact on the power curve, while the other relevant process parameters rather affect the respective level of power consumption. Second, the energy consumption of the laser generator dominates the energy consumption of the entire HS DED-LB system, with a share of approx. 41%, 57%, and 62% in three build tasks. Third, the proposed UPLCI is a powerful tool for estimating the energy requirement for producing representative parts. For all three parts studied, a maximum deviation of only 3% between the calculated and the measured total energy demand was obtained.

In the following steps, the model will be improved by increasing the level of detail. For this purpose, the focus

is put on the two units with the highest energy demand, the laser, and the trajectory system. In addition, further investigations of the suction unit and its fluctuations will be carried out. It is also planned to integrate the here presented model into a part's entire production chain. Accordingly, basic models for raw material extraction, powder production and post-processing steps will be developed at a later stage.

The UPLCI model presented here is part of the effort to develop a database of reusable models and calculation tools to analyze the energy demand and resource requirements of major manufacturing processes, to thus estimate their environmental impacts. It can also be linked to other models of the series, e. g., to represent post-processing.

Data availability All data reported in this manuscript are available from the corresponding author upon request.

Declarations

Conflict of interest The authors declare that they have no conflict of interest.

References

1. Kellens K, Baumers M, Gutowski TG, Flanagan W, Lifset R, Duflou JR (2017) Environmental dimensions of additive manufacturing: mapping application domains and their environmental implications. J Ind Ecol 21:49–68
2. Kellens K, Mertens R, Paraskevas D, Dewulf W, Duflou JR (2017) Environmental impact of additive manufacturing processes: Does am contribute to a more sustainable way of part manufacturing? Procedia CIRP 61:582–587
3. Bambach MD, Bambach M, Sviridov A, Weiss S (2017) New process chains involving additive manufacturing and metal forming—a chance for saving energy? Procedia Eng 207:1176–1181
4. Ma K, Smith T, Lavernia EJ, Schoenung JM (2017) Environmental sustainability of laser met-al deposition: the role of feedstock powder and feedstock utilization factor. Procedia Manuf. https://doi.org/10.1016/j.promfg.2016.12.049
5. Gu DD, Meiners W, Wissenbach K, Poprawe R (2012) Laser additive manufacturing of metallic components: materials, processes and mechanisms. Int Mater Rev 57:133–164
6. DIN Normenausschuss Werkstofftechnologie (NWT) (2017) Additive Fertigung - Grundlagen – Terminologie (ISO/ASTM 52900:2017 (D))
7. Le Bourhis F, Kerbrat O, Hascoet J-Y, Mognol P (2013) Sustainable manufacturing: evaluation and modeling of environmental impacts in additive manufacturing. Int J Adv Manuf Technol 69:1927–1939
8. Le Bourhis F, Kerbrat O, Dembinski L, Hascoet J-Y, Mognol P (2014) Predictive model for environmental assessment in additive manufacturing process. Procedia CIRP 15:26–31
9. Serres N, Tidu D, Sankare S, Hlawka F (2011) Environmental comparison of MESO-CLAD® process and conventional machining implementing life cycle assessment. J Clean Prod 19:1117–1124
10. Jiang Q, Liu Z, Li T, Cong W, Zhang H-C (2019) Emergy-based life-cycle assessment (Em-LCA) for sustainability assessment: a case study of laser additive manufacturing versus CNC machining. Int J Adv Manuf Technol. https://doi.org/10.1007/s00170-019-03486-8
11. Xiong Y, Lau K, Zhou X, Schoenung JM (2008) A streamlined life cycle assessment on the fabrication of WC–Co cermets. J Clean Prod. https://doi.org/10.1016/j.jclepro.2007.05.007
12. Wilson JM, Piya C, Shin YC, Zhao F, Ramani K (2014) Remanufacturing of turbine blades by laser direct deposition with its energy and environmental impact analysis. J Clean Prod 80:170–178
13. Liu Z, Jiang Q, Cong W, Li T, Zhang H-C (2018) Comparative study for environmental performances of traditional manufacturing and directed energy deposition processes. Int J Environ Sci Technol 15:2273–2282
14. Jackson MA, van Asten A, Morrow JD, Min S, Pfefferkorn FE (2016) A comparison of energy consumption in wire-based and powder-based additive-subtractive manufacturing. Procedia Manuf. https://doi.org/10.1016/j.promfg.2016.08.087
15. Wippermann A, Gutowski TG, Denkena B, Dittrich M-A, Wessarges Y (2020) Electrical energy and material efficiency analysis of machining, additive and hybrid manufacturing. J Clean Prod 251:119731
16. Overcash M, Twomey J, Kalla D Unit process life cycle inventory for product manufacturing operations. https://doi.org/10.1115/MSEC2009-84065.
17. Zhang H, Zhao F (2019) Reusable unit process life cycle inventory for manufacturing: gas metal arc welding. Prod Eng Res Devel. https://doi.org/10.1007/s11740-018-0869-1
18. Linke B, Overcash M (2017) Reusable unit process life cycle inventory for manufacturing: grinding. Prod Eng Res Devel. https://doi.org/10.1007/s11740-017-0768-x
19. Raoufi K, Harper DS, Haapala KR (2020) Reusable unit process life cycle inventory for manufacturing: metal injection molding. Prod Eng Res Devel. https://doi.org/10.1007/s11740-020-00991-8
20. Simon T, Yang Y, Lee WJ, Zhao J, Li L, Zhao F (2019) Reusable unit process life cycle inventory for manufacturing: stereolithography. Prod Eng Res Devel. https://doi.org/10.1007/s11740-019-00916-0
21. Ramirez-Cedillo E, García-López E, Ruiz-Huerta L, Rodriguez CA, Siller HR (2021) Reusable unit process life cycle inventory (UPLCI) for manufacturing: laser powder bed fusion (L-PBF). Prod Eng Res Devel. https://doi.org/10.1007/s11740-021-01050-6
22. Schaible J, Sayk L, Schopphoven T, Schleifenbaum JH, Häfner C (2021) Development of a high-speed laser material deposition

process for additive manufacturing. J Laser Appl. https://doi.org/10.2351/7.0000320

23. Ehmsen S, Glatt M, Aurich JC (2023) Influence of process parameters on the power consumption of high-speed laser directed energy deposition. Procedia CIRP 116:89–94. https://doi.org/10.1016/j.procir.2023.02.016